Advanced Composite Materials
Publication details, including instructions for authors and subscription information:
http://www.tandfonline.com/loi/tacm20

A study on residual stresses in polymer composites using moiré interferometry

Krishnakumar Shankar , Huimin Xie , Riyu Wei , Anand Asundi & Chai Gin Boay

Version of record first published: 02 Apr 2012.

To cite this article: Krishnakumar Shankar , Huimin Xie , Riyu Wei , Anand Asundi & Chai Gin Boay (2004): A study on residual stresses in polymer composites using moiré interferometry, Advanced Composite Materials, 13:3-4, 237-253

To link to this article: http://dx.doi.org/10.1163/1568551042580181

Adv. Composite Mater., Vol. 13, No. 3-4, pp. 237–253 (2004)

Also available online - www.vsppub.com

A study on residual stresses in polymer composites using moiré interferometry

KRISHNAKUMAR SHANKAR [1], HUIMIN XIE [2,*], RIYU WEI [3], ANAND ASUNDI [4] and CHAI GIN BOAY [4]

[1] *University College, University of New South Wales, Australian Defence Force Academy, Canberra, ACT 2600 Australia*
[2] *Department of Engineering Mechanics, Tsinghua University, 100084 Beijing, China*
[3] *Advanced Computational Modelling Centre, The University of Queensland, Australia*
[4] *School of Mechanical and Production Engineering, Nanyang Technological University, Singapore*

Received 25 September 2003; accepted 23 July 2004

Abstract—Moiré interferometry is applied along with the hole drilling technique to determine residual cure stresses in symmetric cross ply graphite epoxy laminates. Traditional moiré interferometry set-up using two collimated angle beams was employed to provide the virtual reference grating while a cross grating with a frequency of 1200 lines per mm was replicated on the specimen surface. Holes of different depths, each one penetrating one additional layer of the laminate, were drilled using a high speed air turbine drill to relieve the stresses in each layer sequentially. The strain distribution around each hole was computed from correlation of the undistorted carrier fringe pattern with the distorted fringe patterns around the holes. The measured strain distributions are compared to residual strain distributions by finite element analysis.

Keywords: Residual stress; composites; moiré interferometry.

1. INTRODUCTION

Fiber reinforced polymer composite laminates have found numerous applications in aircraft construction due to their higher strength and stiffness-to-weight ratios compared to metallic materials. However, a major drawback which limits the utilization of their full capabilities is the accumulation of residual stresses within the layers of the composite during the cure process at high temperatures. These residual stresses arise from the differential thermal expansion between layers oriented at different angles within the laminate and can be as high as sixty percent of the material's transverse strength. The traditional method of measuring residual stresses

*To whom correspondence should be addressed. E-mail: xiehm@mail.tsinghua.edu.cn

are either destructive involving cutting the specimen into pieces, i.e. sectioning, or semi-destructive, involving drilling holes in the specimen. In either case the removal of material relieves the residual stresses in the specimen due to the creation of free edges. The reduction in stresses can be monitored either using traditional techniques such as photoelasticity or the measurement of localized strain variations using residual stress gauges [1, 2]. Recently, optical techniques have been employed in conjunction with sectioning and hole-drilling techniques to measure residual stresses; these have the advantages of being employable to opaque materials as well as being whole field techniques. The measurement of residual stresses due to welding, interference fits and manufacturing processes in metals have been performed using optical techniques such as holographic interferometry [3–5], coherent optics techniques [6], moiré interferometry [7] and electronic speckle interferometry [8]. Residual stress measurements using moiré interferometry with sectioning techniques have also been reported elsewhere [9, 10]. The application of moiré interferometry in conjunction with hole drilling to measure residual stresses in unsymmetric composite laminates was reported recently [11]. This paper describes the application of moiré interferometry and hole drilling method for measurement of residual stresses in symmetric graphite epoxy laminates.

2. EXPERIMENTAL SET-UP

Figure 1a shows the principle of a typical moiré interferometer with a specimen grating exposed to a two-beam interference system. A He–Ne laser ($\lambda = 6328$ Å) is employed to create the virtual reference grating. The incident angles of the two beams are adjusted so as to provide a reference grating with a frequency that is exactly twice the frequency of the specimen grating (with He–Ne laser an angle of 49.4 degrees generates a virtual reference grating of 2400 lines/mm). When the two incident light beams strike the specimen grating, this grating will diffract the incident light into different beams (with different diffractive orders). In the experiment, when the grating is undeformed, the -1 and $+1$ diffraction orders from the beams emerge perpendicular to the grating, and a null moiré pattern is generated. When the specimen is deformed, the -1 and $+1$ orders will exit the specimen grating warped and interfere with each other. The result is a moiré fringe pattern which represents the displacement component in y axis. In this study, a four-beam moiré interferometer (manufactured by the Beijing Holo Tech Co., China) is utilized (see Fig. 1b), which allows us to measure the displacement components in y and z axis simultaneously.

The specimens were fabricated from graphite epoxy Hercules AS4/3501 using a cure temperature of 175 degrees Celsius, vacuum and pressure application as per the manufacturer's specifications. Two laminate configurations were constructed: a 16 layer uni-directional lay up, and a symmetric cross-ply laminate of (0, 90, 90, 0) lay-up where each ply consisted of 4 layers of approximately 0.125 mm thick unidirectional prepreg. Thus both laminates had a thickness of approximately 2 mm.

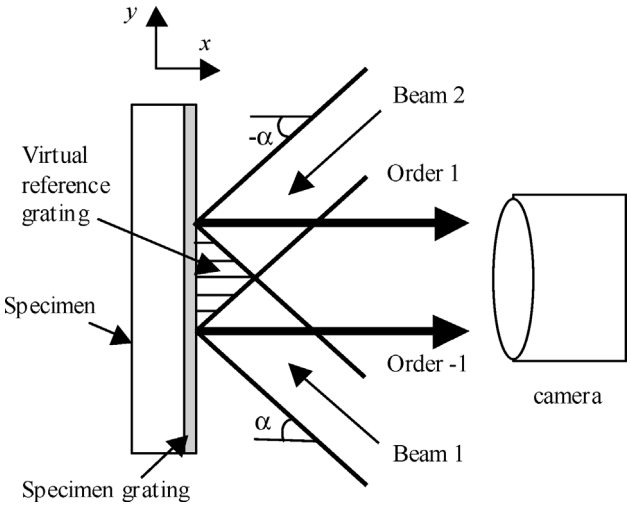

(a)

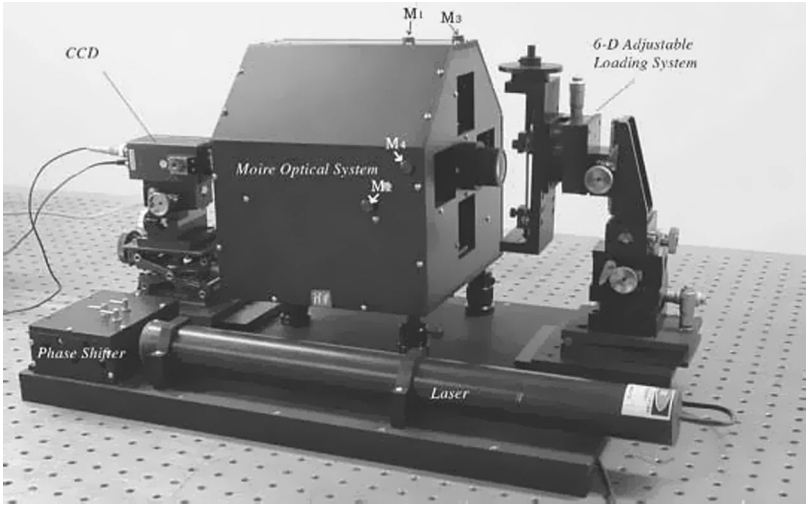

(b)

Figure 1. (a) Principle of moiré interferometry. (b) A photograph of four-beam moiré interferometry set-up.

They were cut to 70 mm × 35 mm rectangular panels to provide specimens for the study. Unfortunately, a period of about 18 months elapsed between the specimen construction and their use in the residual stress measurement experiments. While this may have caused some relaxation of the residual stresses in the laminates, it provided a more realistic simulation of the situation that may be expected in composites after a few years of service. Diffraction gratings with a 1200 lines per mm were replicated on the specimen surface.

For replication, first a master grating is recorded on a glass holographic plate using interference between two collimated beams of coherent light. When the photographic plate is developed its emulsion coating develops ridges corresponding to the dark and bright patterns of the recorded grating. Using vacuum deposition technique, a thin layer of aluminium is coated on to the holographic plate, where it settles into the ridges in the emulsion layer forming a true replica of the grating. The grating mold (glass plate) is then bonded on to the specimen surface using epoxy adhesive (taking care not to trap any air bubbles between them). When the glass mold is separated from the specimen surface after the adhesive is cured (at room temperature), the aluminium lines are left on the specimen surface providing an exact replica of the master grating. In the current work a specimen grating of 1200 lines/mm was replicated on the composite specimens. A matching reference grating frequency of 2400 lines/mm employed in the moiré interferometry set-up provided a sensitivity of 0.417 microns of in-plane displacement per fringe.

For the experiment, the specimen was mounted on a rigid frame and drilled with an air turbine drill bit of 1.6 mm diameter mounted on a rigid platform. It is to be noted that drilling with a normal drill will produce a blind hole with a conical bottom having an included angle of 118 degrees, which was considered acceptable for this study, but a 'slot drill' may be employed to produce blind holes with nearly perfect flat faces at the bottom. The moiré fringe patterns were viewed through a high magnification lens through a CCD camera and recorded digitally into a PC based computer for later processing.

3. RESIDUAL STRESSES FROM CLASSICAL LAMINATE THEORY

Assuming that the consolidation of the layers during cure occurred at 175°C and that the day-time room temperature at which the tests were performed was 25°C, the thermal and mechanical strains and residual stresses for the cross-ply laminates can be determined using classical laminate plate theory [12] for a known temperature difference ΔT as follows.

The stiffness coefficient matrix $[\bar{Q}]$ for a zero degree lamina can be obtained in terms of the lamina material properties as follows:

$$\left[\bar{Q}\right]_0 = \begin{bmatrix} Q_{11} & Q_{12} & 0 \\ Q_{12} & Q_{22} & 0 \\ 0 & 0 & Q_{66} \end{bmatrix} = \frac{1}{(1-\nu_{12}\nu_{21})} \begin{bmatrix} E_{11} & \nu_{12}E_{22} & 0 \\ \nu_{12}E_{22} & E_{22} & 0 \\ 0 & 0 & G_{12} \end{bmatrix}, \quad (1)$$

where E_{11} and E_{22} represent the elastic moduli in the fiber direction and transverse direction respectively, ν_{12} and G_{12} are the Poisson's ratio and the shear modulus in the 12 direction. The same relations hold good for a ninety degree lamina except the coefficients Q_{11} and Q_{22} replace each other. $\{\alpha\}_k$, the vector of thermal expansion

coefficients for the zero and ninety degree layers are respectively given by

$$\left\{\begin{array}{c}\alpha_x\\ \alpha_y\\ \alpha_{xy}\end{array}\right\}_0 = \left\{\begin{array}{c}\alpha_{11}\\ \alpha_{22}\\ 0\end{array}\right\}, \quad \left\{\begin{array}{c}\alpha_x\\ \alpha_y\\ \alpha_{xy}\end{array}\right\}_{90} = \left\{\begin{array}{c}\alpha_{22}\\ \alpha_{11}\\ 0\end{array}\right\}. \tag{2}$$

The effect of thermal loading caused by the temperature difference can be expressed in terms of resultant thermal forces $\{N^T\}$ acting on the laminate as:

$$\left\{N^T\right\} = (\Delta T)\sum_{k=1}^{n}\left[\bar{Q}\right]_k \{\alpha\}_k\, t_k, \tag{3}$$

where n is the total number of plies and t_k is the individual ply thickness. It may be noted that the resultant thermal moments vanish due to symmetry of the laminates under consideration. The resultant laminate strains $\{\varepsilon^0\}$ being uniform across the thickness for symmetric laminates, are then given by

$$\left\{\begin{array}{c}\varepsilon_x^0\\ \varepsilon_y^0\\ \gamma_{xy}^0\end{array}\right\} = A^{-1}\left\{\begin{array}{c}N_x^T\\ N_y^T\\ N_{xy}^T\end{array}\right\}, \tag{4}$$

where A^{-1} is the inverse of the laminate in-plane stiffness matrix A, whose elements A_{ij} (for $i, j = 1, 2, 3$) are given by

$$A_{ij} = \sum_{k=1}^{N}(\bar{Q}_{ij})_k t_k. \tag{5}$$

The mechanical strains required to maintain continuity of the total strains across the laminate is given by the difference between the total strains and the thermal strains in each individual layer ($k = 1, 2, 3$)

$$\left\{\varepsilon^M\right\}_k = \left\{\varepsilon^0\right\} - \left\{\varepsilon^T\right\}_k = \left\{\varepsilon^0\right\} - \Delta T\,\{\alpha\}_k\,. \tag{6}$$

The residual stresses in the individual layers required to maintain these mechanical strains may then be obtained from

$$\left\{\begin{array}{c}\sigma_x\\ \sigma_y\\ \tau_{xy}\end{array}\right\}_k = \left[\bar{Q}\right]_k \left\{\varepsilon^M\right\}_k. \tag{7}$$

For a symmetric four-ply laminate (0, 90, 90, 0), the thermal forces given by equation (3) are reduced to $N_x^T = N_y^T = N_0^T$ and $N_{xy}^T = 0$, where

$$N_0^T = 2t_k(\Delta T)\left[Q_{11}\alpha_{11} + Q_{22}\alpha_{22} + Q_{12}(\alpha_{11} + \alpha_{11})\right], \tag{8}$$

and the laminate mid-plane strains given by equation (4) are reduced to $\varepsilon_x^0 = \varepsilon_y^0 = \varepsilon_0$ and $\gamma_{xy}^0 = 0$, where

$$\varepsilon_0 = (\Delta T)\left[\frac{Q_{11}\alpha_{11} + Q_{22}\alpha_{22} + Q_{12}(\alpha_{11} + \alpha_{22})}{Q_{11} + Q_{22} + 2Q_{12}}\right] = (\Delta T)\alpha_0. \tag{9}$$

Table 1.
Strain and stress distribution in (0/90/90/0) CFRP laminate due to cure

$\Delta T = -150°C$	Total strain (micro-strain)	Free state thermal strain (micro-strain)	Residual strain (micro-strain)	Residual stress (MPa)
Zero degree ply (x direction)	−280.7	45	−325.7	−34.6
Zero degree ply (y direction)	−280.7	−4215	3934.3	34.6
Ninety deg ply (x direction)	−280.7	−4215	3934.3	34.6
Ninety deg ply (y direction)	−280.7	45	−325.7	−34.6

The residual (mechanical) strains in the zero and ninety degree plies can now be obtained from equation (6) as

$$\left\{ \begin{array}{c} \varepsilon_x^M \\ \varepsilon_y^M \\ \gamma_{xy}^M \end{array} \right\}_0 = \left\{ \begin{array}{c} \varepsilon_y^M \\ \varepsilon_x^M \\ \gamma_{xy}^M \end{array} \right\}_{90} = \Delta T \left\{ \begin{array}{c} \alpha_0 - \alpha_{11} \\ \alpha_0 - \alpha_{22} \\ 0 \end{array} \right\}, \tag{10}$$

and the residual stresses in the zero and ninety degree plies may be obtained from equation (7) as

$$\left\{ \begin{array}{c} \sigma_x \\ \sigma_y \\ \tau_{xy} \end{array} \right\}_0 = \left\{ \begin{array}{c} \sigma_y \\ \sigma_x \\ \tau_{xy} \end{array} \right\}_{90} = \Delta T \left\{ \begin{array}{c} Q_{11}(\alpha_0 - \alpha_{11}) + Q_{12}(\alpha_0 - \alpha_{22}) \\ Q_{12}(\alpha_0 - \alpha_{11}) + Q_{22}(\alpha_0 - \alpha_{22}) \\ 0 \end{array} \right\}. \tag{11}$$

Substituting for Q_{ij}'s and α_0, equation (11) can be simplified to determine the residual stresses in the zero and ninety degree plies as:

$$(\sigma_x)_0 = (\sigma_y)_{90} = -(\sigma_y)_0 = -(\sigma_x)_{90} = (\Delta T)\left[\frac{E_{11}E_{22}(\alpha_{22} - \alpha_{11})}{E_{11} + E_{22} + 2\nu_{12}E_{22}}\right]. \tag{12}$$

The engineering properties of the graphite epoxy AS4/3501 material obtained from literature [13] and employed in the analysis were: $E_{11} = 138$ GPa, $E_{22} = 8.96$ GPa, $G_{12} = 7.1$ GPa, $\nu_{12} = 0.3$. The coefficients of thermal expansions (CTE) parallel and perpendicular to the fibers are equal to [13] $\alpha_{11} = -0.3 \times 10^{-6}$ and $\alpha_{22} = 28.1 \times 10^{-6}$ mm/mm/degree Kelvin, respectively. The results for the total strains, thermal strains, residual (mechanical) strains and the residual stresses obtained from equations (9) to (12) above for a temperature change ΔT of 150°C and the above material properties are presented in Table 1. It may be noted that since the CTE in the fiber direction is negative, the layers actually tend to expand a little upon cooling in the x direction (zero degree direction of the outer layers shown in Fig. 2), while the ninety degree layers tend to contract to a much higher extent. For the final strain to be the same in all the layers (-281 $\mu\varepsilon$), high tensile residual strains are introduced in the transverse direction (3934 $\mu\varepsilon$), while the compressive

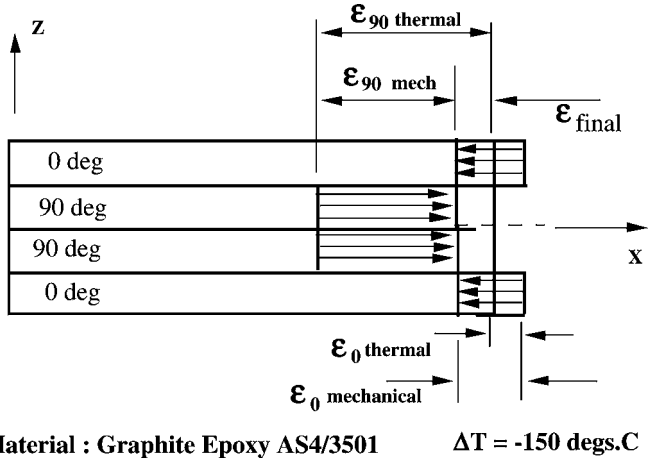

Figure 2. Thermal and residual mechanical strains due to cure in a symmetric cross-ply CFRP laminate.

mechanical strain parallel to the fiber reinforcement is an order of magnitude lower ($-326\ \mu\varepsilon$). The residual stress in the transverse direction is 34.6 MPa tensile, which is 67% of the transverse tensile strength of the CFRP material (52 MPa). It is to be noted that the same stresses and strains will exist along the fiber direction and perpendicular to it in a (90, 0, 0, 90) laminate, considering the difference between this and a (0, 90, 90, 0) laminate is only a rotation of the coordinate axes by ninety degrees.

4. EXPERIMENTAL RESULTS WITH THE MOIRÉ INTERFEROMETRY

Each of the three specimens, unidirectional, $(0,90)_{sym}$ and $(90/0)_{sym}$ were examined with at least four different holes drilled in them, with depths ranging from 0.5 mm to 2 mm (full thickness). It was found that there were virtually no changes in the fringe patterns observed for each configuration once the hole depth was about a quarter of the thickness, i.e. at least reached the first major interface. Typical fringe patterns obtained from the moiré interferometry set up are displayed in Figs 3 to 5. It may be noted that the alignment between the virtual grating and the specimen grating was arranged so as to provide a carrier fringe pattern of reasonable frequency. When there are no local variations in the strain distribution, the carrier fringes remain parallel indicating a constant change in displacement across the width of the plate surface. Since it is known that the fringes remote from the hole will be unaffected by the release of residual stresses at the edge of the hole, the deviation of the fringe lines in the vicinity of the hole can be compared to the uniform fringes away from the hole (carrier fringes) to map the relative displacement due to the residual strains released at the hole.

Figures 3a and 3b show the fringes generated by the U and V displacement fields (parallel to the fibers and perpendicular to the fibers) in the unidirectional laminate

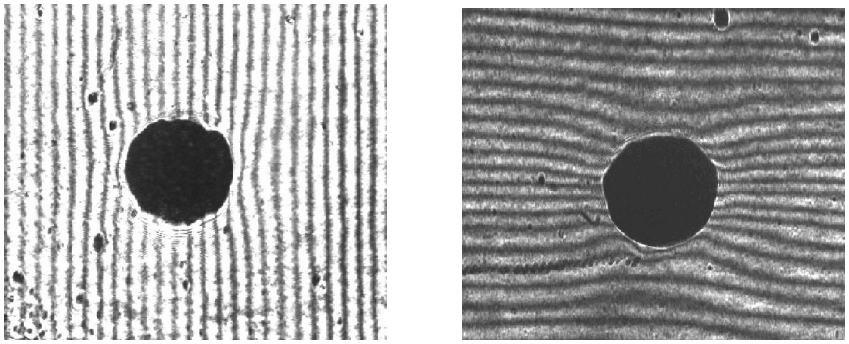

(a) (b)

Figure 3. Unidirectional CFRP plates with (a) U displacement fringes, (b) V displacement fringes.

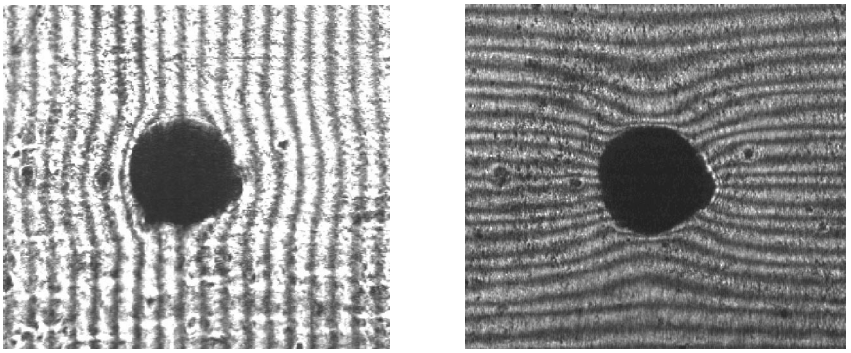

(a) (b)

Figure 4. (0/90/90/0) CFRP plate with 1.6 mm diameter hole (a) U displacement fringes, (b) V displacement fringes.

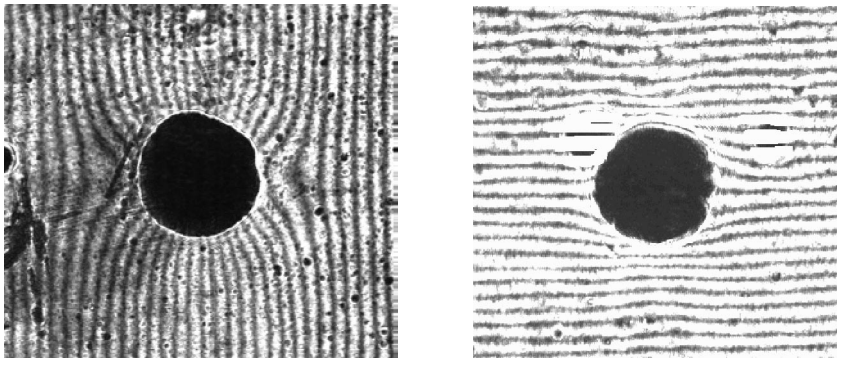

(a) (b)

Figure 5. (90/0/0/90) CFRP plate with 1.6 mm diameter hole (a) U displacement fringes, (b) V displacement fringes.

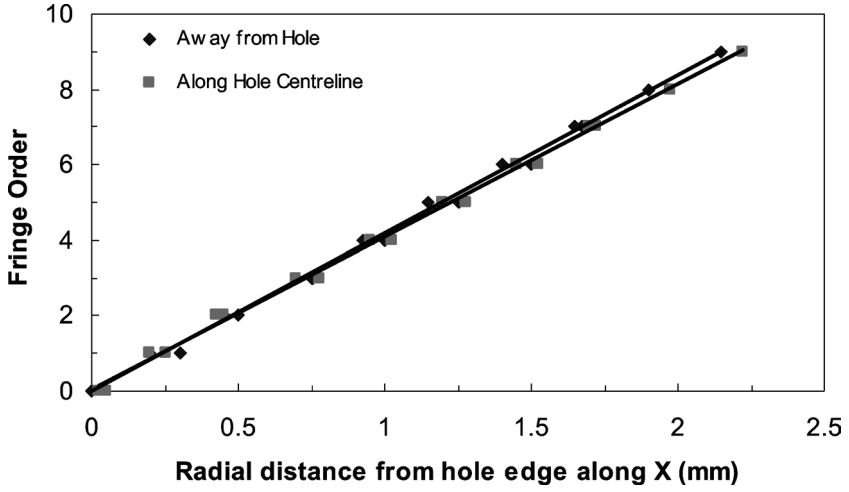

(a)

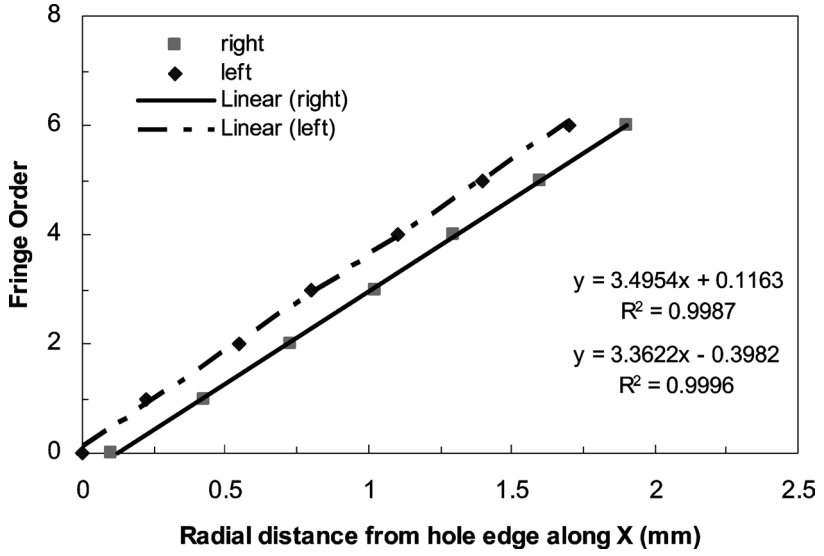

(b)

Figure 6. (a) Plot of U displacement fringe orders along center line of hole in unidirectional laminate. (b) Plot of U displacement fringe orders along center line of hole in (0/90/90/0) laminate.

with a through-thickness hole and a 1.5 mm deep hole, respectively. It can be seen that the fringes show little distortion in the vicinity of the hole indicating the lack of (released) residual strains in this laminate. The U displacement fringe orders along the hole centre line and away from the hole in Fig. 3a are plotted together in Fig. 6a for comparison. It is seen that in both cases the distribution is linear, hence there are no local strains in the vicinity of the hole. Figures 4a and 4b respectively depict the fringe patterns corresponding to U and V displacement

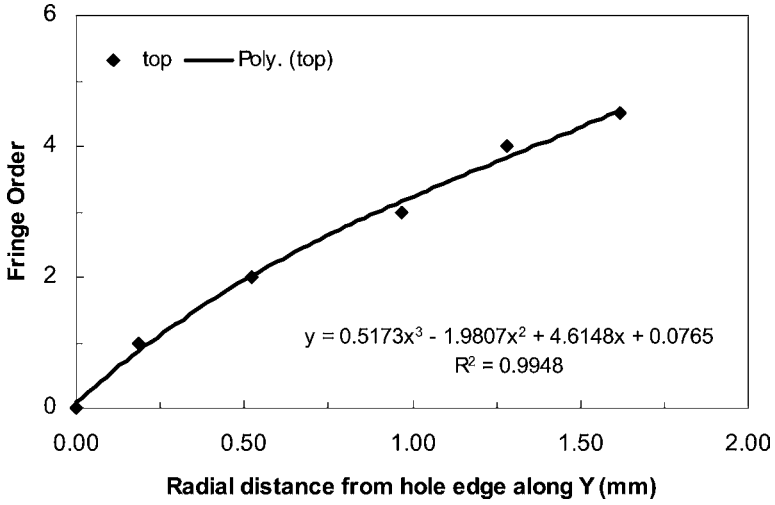

(a)

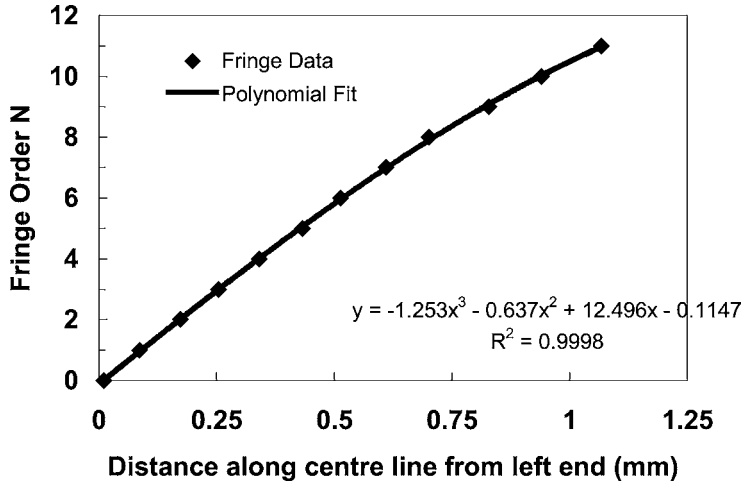

(b)

Figure 7. (a) Plot of V displacement fringe orders along center line of hole in (0/90/90/0) laminate. (b) Plot of U displacement fringe orders along center line of hole in (90/0/0/90) laminate.

fields (parallel and perpendicular to the fibers, respectively) on the surface of the (0/90/90/0) laminate, while Figs 5a and 5b respectively depict the fringe patterns corresponding to U (perpendicular to the fibers, in this case) and V (parallel to the fibers) displacement fields on the surface of (90/0/0/90) laminates with 1 mm deep holes. It is evident that in both cases the fringe patterns of displacements parallel to the fibers (U in Fig. 4a and V in Fig. 5b) show only small deviations from their remote patterns, indicating virtually no local strains as evidenced by the linearity of the U displacement fringe orders along center line of hole in (0/90/90/0)

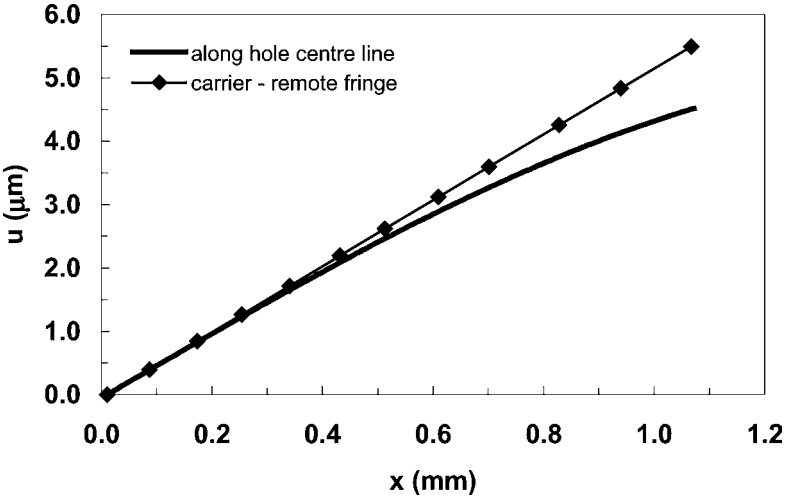

Figure 8. U displacements along center line of hole in (90/0/0/90) laminate.

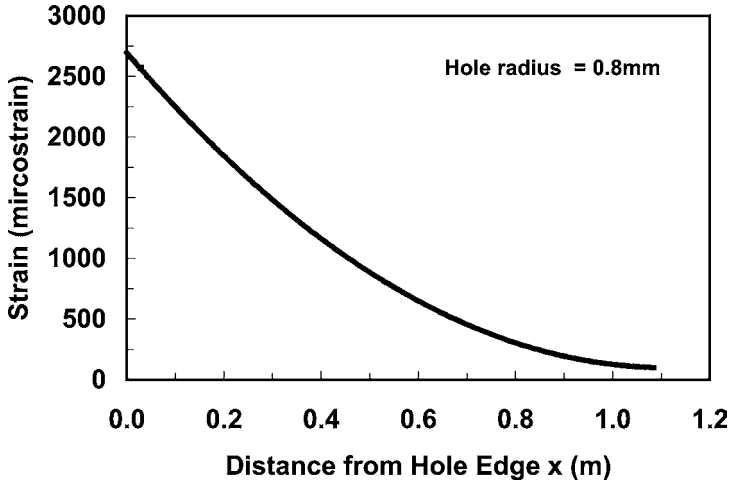

Figure 9. Residual strain in *X* direction along centre line in (90/0/0/90) laminate.

laminate plotted in Fig. 6b. In contrast, the fringes generated by displacements perpendicular to the fibers show considerable distortions. The V displacement fringes from Fig. 4b and the U displacement fringes from Fig. 5a are plotted in Figs 7a and 7b respectively against their locations along the center-line of the hole. The fringe numbers start at an arbitrary point at a distance remote from the hole where the fringes appear uniform. These displacement variations are no longer linear, indicating the presence of significant relative transverse strains in the vicinity of the hole. The third order polynomials fitted to the curves (displayed in the Figs 7a and 7b) have an R^2 value very close to 1, indicating the accuracy of the curve fit.

The fringe data can be converted to axial displacement using the relationship $U = N/f$ where N is the fringe order and f is the reference grating frequency (2400 lines/mm). The actual displacement distribution caused by the release of the stresses due to hole drilling is obtained by subtracting the apparent linear displacements of the carrier fringes from the third order polynomials fitted to the displacement data along the hole centre line. The residual strains are then given by the spatial derivatives of these displacement distributions. To illustrate the procedure of the determination of the residual strains, the U displacements of the (90/0/0/90) laminate in Fig. 5a calculated from the fringe orders plotted in Fig. 7b are shown in Fig. 8 along with the displacement distribution of the carrier fringes away from the hole. Figure 9 is a plot of the distribution of the released residual strains in the X direction, i.e. in the transverse direction of fiber reinforcement for the (90/0/090) laminate along the diameter starting from the edge of the hole, obtained by numerical differentiation of the difference between the two displacement plots in Fig. 8. The maximum strain occurs at the edge of the hole and is equal to 2720 $\mu\varepsilon$. It may be noted that the released strain values drop steeply to almost zero within a distance of about 1 mm (less than 1.5 times the radius of the hole or 0.6 times the thickness of the laminate).

5. COMPARISON WITH FINITE ELEMENT ANALYSIS

The classical laminate plate theory only allows the analysis of residual strains that can be measured with a small hole extending over the full thickness of the laminate. In order to investigate the stress and strain distributions in plates with part-through holes and for the purpose of comparison with experimental results, part-through and through-thickness holes in the four-ply laminate were modeled using finite element analysis. The finite element model created using ANSYS software employed three-dimensional brick elements. The FE model represented a symmetric quarter of the laminate centred about the drilled hole and spread up to 10 times the radius of the hole. Sixteen elements were employed across the thickness of the laminate, with one element per ply, i.e. four elements per layer of material with the same fiber orientation. In the plane of the laminate, a fine mesh was employed with sixteen elements in the circumferential direction and sixteen elements across the radius in the vicinity of the hole. The density of the mesh was gradually reduced in regions further away from the hole. In all, a typical quarter model of the laminate contained over 12 000 brick elements. Since the FE model was being subjected to pure thermal loading, only boundary conditions constraining rigid body movements (translation and rotation) along the lines of symmetry were applied on the model. Thus the laminate was free to expand along the plane as well as in the transverse direction under the thermal loading. In the FE analysis, a (90/0/0/90) laminate with the same material properties as indicated in the foregoing classical laminate theory was modeled with a circular hole of the same dimension as employed in the experiments.

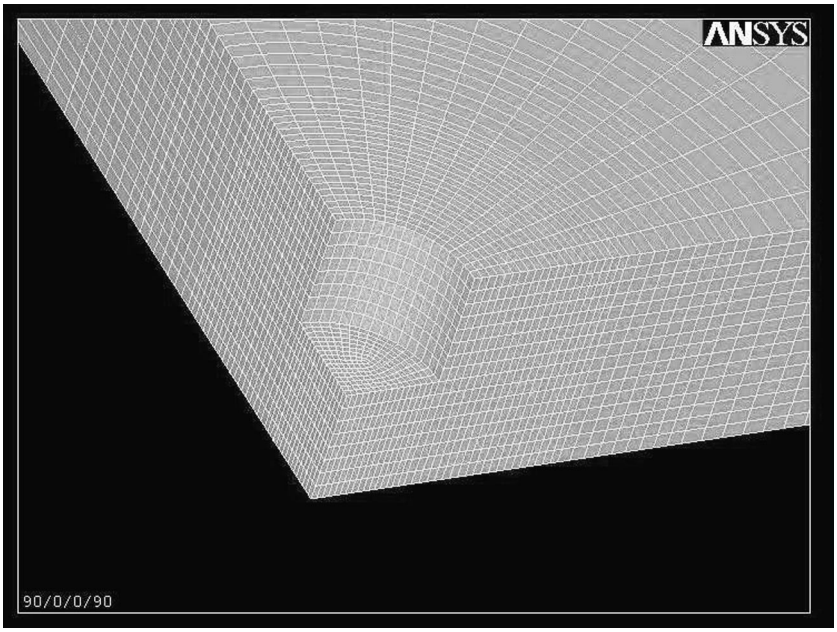

Figure 10. Finite element mesh for half-depth hole.

It is to be noted that, as with the classical laminate theory, in a finite element model, the (90/0/0/90) laminate differs from the (0/90/90/0) only in that the coordinate system is rotated by 90 degrees; hence the results obtained in the X direction for one configuration will be identical to those for the other laminate in the Y direction and *vice versa*. The plate was then subjected to thermal loading of $-150°$C and the stresses analysed under the assumption that the thermal stresses at the free edge of the hole due to the temperature change will be the same as the residual stresses in a plate cured at high temperature and released by drilling a hole after going through the same temperature differential. Figure 10 shows the finite element mesh in the vicinity of a hole extending over half the depth of the laminate. The distribution of thermal stresses in the X direction (horizontal axis) along the edges of the plate, along the edge of the part through hole and on the surface of the top ply is shown in Fig. 11a. Figure 11b shows the stress distribution in X direction (horizontal) in a plate with a through-the-thickness hole for the same temperature differential of $-150°$C. Keeping in mind that the outer plies have fibers oriented transverse to the stress direction (X-axis), while inner two plies have fibers running parallel to the X axis, the stresses in regions of the plates away from the holes (Figs 11a and 11b) are in excellent agreement with the magnitudes $+35$ MPa for the 90 degree ply and -35 MPa for the zero degree ply predicted by classical laminate theory. Whereas, in the three-dimensional finite element analysis, the local stress values at the edges of the holes exhibit considerable variation in both cases. It it to be noted that Kirchhoff's assumption of plane sections remaining plane no longer hold good in the 3D analysis. As can be seen in Fig. 11b, the outer 90 degree layers are able

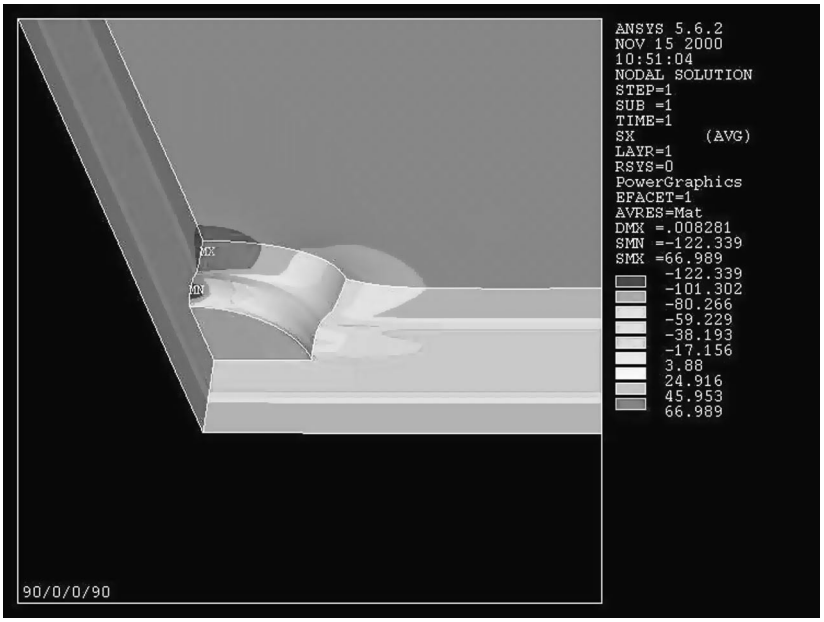

(a)

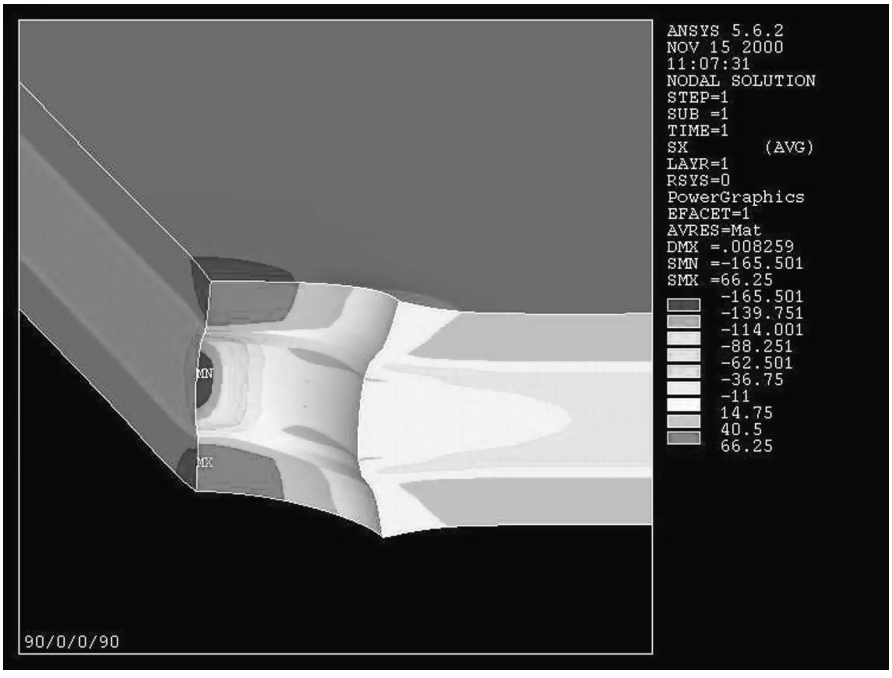

(b)

Figure 11. (a) Residual stress distribution in *X* direction for half-depth hole in (90/0/0/90) laminate. (b) Residual stress distribution in *X* direction for full-depth hole in (90/0/0/90) laminate.

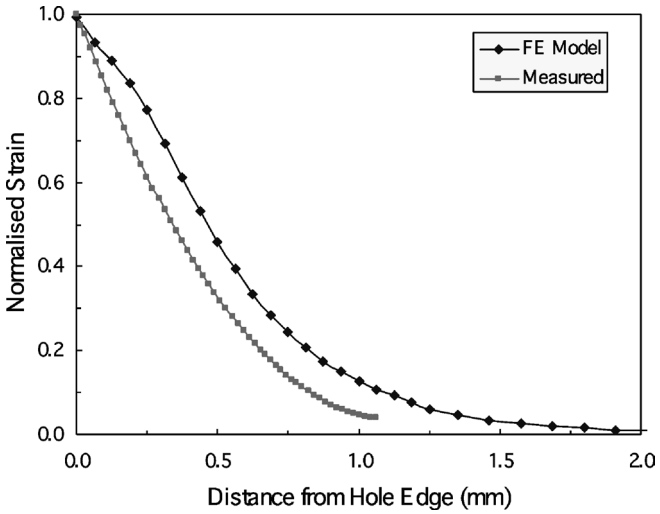

Figure 12. Comparison of measured and predicted normalised residual strains in X direction on surface for full depth hole in (90/0/0/90) laminate.

to remain deformed to a larger extend in the transverse direction (X direction) than the inner zero degree layers, deforming the hole into a horizontally stretched ellipse in the outer layers and a vertically stretched ellipse in the inner layers. Further, the stresses normal to the edge of the hole vanish all along its boundary, while stresses in the tangential direction exhibit an increase in magnitude. The stress concentrations in the tangential direction along the hole boundary are about 1.9 and 3.5 for the 90 degree plies and the zero degree plies for the part-through hole (Fig. 11a) and 1.9 and 4.7 for the 90 degree plies and the zero degree plies for the through-thickness hole (Fig. 11b), respectively. It is significant to note that the magnitude of maximum stresses on the upper surface of the ninety degree ply is the same for both the through-thickness hole and the part-through hole. This explains the similarity in the more fringe patterns and the measured residual strains for plates with full holes and part-through holes.

Figure 12 shows a comparison of the residual strain distributions predicted by the finite element model and measured with the moiré interferometry. Note that both strain values are normalized with respect to their maximum values, for clarity of comparison, as the magnitudes of the maximum strains are different due to reasons mentioned above.

6. DISCUSSION AND CONCLUSION

The residual stresses due to the high temperature curing process in laminated cross-ply graphite epoxy coupons were measured experimentally using moiré interferometry in conjunction with hole drilling. The replication of the diffraction grating on the specimen and alignment of the optical set-up for moiré interferometry require

considerable expertise and skill; both of these were conducted by researchers at NTU. The use of hole drilling as opposed to sectioning in conjunction with moiré interferometry offers the facility of employing fringes remote from the drilled hole as carrier fringes for comparison. This eliminates the need for taking double exposures, as well as that of creating and recreating a null field at the image plane before and after releasing the stresses, which can occupy considerable effort and time.

The maximum value of the residual strain the CFRP material was measured to be 2720 $\mu\varepsilon$, which is about 30% lower than the 3934 $\mu\varepsilon$ predicted by classical laminate plate theory. It is felt that the discrepancy may be due primarily to the relaxation of residual stresses in the material due to aging, since the residual stress measurements were conducted about 18 months after the laminates were manufactured. There could also have been some relaxation of the stresses due to humidity in the test environment at the NTU laboratory. Factors such as variations in the actual material and thermal properties as opposed to the theoretical values employed in the calculations and experimental errors may also have contributed. It is also to be noted that the predictions are based on two linear elastic plate theory, which ignores the variation of the strains and stresses across the thickness. A more refined analysis using three-dimensional finite element modeling is being carried out at present for comparison with the results from the classical theory. Another factor that has to be considered is the consolidation temperature of the composite at cure. It has been assumed that the consolidation of the layers takes place at the maximum cure temperature (175°C) after which they expand or contract together introducing residual stresses in each other. But it is quite likely that consolidation may take place at a lower temperature, say 20 or 30 degrees below the maximum cure temperature, which would bring the theoretical estimates much closer to the measured values. The fact that the measured residual strain distributions drop steeply and virtually vanish at distances of about one millimeter from the edge of the hole is consistent with findings reported earlier [12] on experimental and theoretical investigations of edge effects.

The measured strain distributions from moiré interferometry are compared to residual strain distributions by finite element analysis, and the results are consistent.

REFERENCES

1. D. Post, B. Han and P. Ifju, *High Sensitivity Moiré*. Springer-Verlag, Berlin (1994).
2. ASTM Standard E837-95, Standard Test Method for Determining Residual Stresses by the Hole-drilling Strain-gage Method (1995).
3. S. T. Lin, *et al*., Two holographic blind-hole methods for measuring residual stresses, *Experimental Mechanics* **34** (2), 141–147 (1994).
4. A. Makino, *et al*., Determination of biaxial residual stresses by a holographic-hole drilling technique, *J. Engng Mater. Technol.* **118** (4), 583–588 (1996).
5. A. Makino and D. V. Nelson, Determination of sub-surface distributions of residual stresses by a holographic-hole drilling techniques, *J. Engng Mater. Technol.* **119** (1), 95–103 (1997).
6. F. M. Furgiuele, *et al*., Measuring residual stresses by hole-drilling and coherent optics techniques: a numerical calibration, *J. Engng Mater. Technol.* **113**, 41–50 (1991).

7. G. Nicoletto, Moiré interferometry determination of residual stresses in the presence of gradients, *Experimental Mechanics* **31** (3), 252–256 (1991).
8. J. B. Zhang, *et al*., Measurement of residual stress using fiber electronic speckle pattern interferometry, in: *Experimental Mechanics, Advances and Applications, Proc. SPIE*, Vol. 2921 (1996).
9. H. E. Gascoigne, Residual surface stresses in laminated cross-ply fiber-epoxy composite materials, *Experimental Mechanics* **34** (1), 270–280 (1994).
10. D. Joh, *et al*., Thermal residual stresses in thick graphite/epoxy composite laminate — uniaxial approach, *Experimental Mechanics* **33** (1), 70–76 (1993).
11. L. Yu, Q. M. Yin and A. Asundi, Residual stresses in unsymmetric laminated carbon fiber composites, in: *Proc. SPIE Int. Soc. Opt. Eng.*, Vol. 3740, pp. 118–121 (1999).
12. R. F. Gibson, *Principles of Composite Material Mechanics*. McGraw-Hill, Singapore (1994).
13. W. T. Tsai, *Theory of Composite Design*. Think Composites, Dayton, Ohio (1992).